Acta Crystallographica Section A
Foundations of Crystallography
ISSN 0108-7673

Received 20 September 2009
Accepted 19 November 2009

Picosecond and femtosecond X-ray absorption spectroscopy of molecular systems

Majed Chergui

Ecole Polytechnique Fédérale de Lausanne, Laboratoire de Spectroscopie Ultrarapide, ISIC, Faculté des Sciences de Base, Station 6, CH-1015 Lausanne, Switzerland. Correspondence e-mail: majed.chergui@epfl.ch

The need to visualize molecular structure in the course of a chemical reaction, a phase transformation or a biological function has been a dream of scientists for decades. The development of time-resolved X-ray and electron-based methods is making this true. X-ray absorption spectroscopy is ideal for the study of structural dynamics in liquids, because it can be implemented in amorphous media. Furthermore, it is chemically selective. Using X-ray absorption near-edge structure (XANES) and extended X-ray absorption fine structure (EXAFS) in laser pump/X-ray probe experiments allows the retrieval of the local geometric structure of the system under study, but also the underlying photoinduced electronic structure changes that drive the structural dynamics. Recent developments in picosecond and femtosecond X-ray absorption spectroscopy applied to molecular systems in solution are reviewed: examples on ultrafast photoinduced processes such as intramolecular electron transfer, low-to-high spin change, and bond formation are presented.

1. Introduction

The advent of femtosecond laser spectroscopy made it possible to observe atomic motions on a timescale that is shorter than a single vibrational period in molecular systems (Zewail, 2000*a*,*b*), giving birth to the field of femtochemistry. In femtosecond spectroscopy, a first (pump) laser pulse excites the system at time zero, while a second (probe) pulse probes the evolution of the system as a function of time delay with respect to the pump pulse. However, optical domain spectroscopy does not deliver molecular structure. Thus, from the early days of femtochemistry, efforts were deployed to implement the traditional structural tools of X-ray and electron diffraction, and of X-ray absorption spectroscopy in time-domain experiments, towards the highest time resolution of picoseconds to femtoseconds.

Most ultrafast structural studies have used X-ray diffraction studying coherent lattice dynamics, strain propagation, melting phenomena and phase transitions in bulk materials and in nanostructures (Rose-Petruck *et al.*, 1999; Siders *et al.*, 1999; Cavalleri & Schoenlein, 2004; Bargheer *et al.*, 2006; Gaffney & Chapman, 2007; Schmizing *et al.*, 2008; Ingold *et al.*, 2008; Johnson *et al.*, 2008). Protein and molecular crystals have also been investigated with 100 ps to ns time resolution (Srajer *et al.*, 1996, 2001; Perman *et al.*, 1998; Ren *et al.*, 2001; Schotte *et al.*, 2003, 2004; Ihee *et al.*, 2005; Lorenc *et al.*, 2009; Collet *et al.*, 2008, 2009), while the first studies at higher temporal resolution are starting to appear (Schmizing *et al.*, 2007). X-ray diffraction of liquids initially proposed by Wilson and co-workers (BenNun *et al.*, 1997; Cao & Wilson, 1998; Bergsma *et al.*, 1986) has so far been limited to the 100 ps resolution (Ihee, 2009; Kim *et al.*, 2009) and is challenging owing to the lack of long-range order and the high background of light scattered by the solvent. The present studies carried out at synchrotrons are, however, crucial as they prepare the ground for the implementation of similar experiments with femtosecond resolution at the new and intense sources of X-rays, such as the X-ray free-electron lasers (XFELs).

Electron diffraction and microscopy have largely demonstrated their power in probing the ultrafast structural dynamics of isolated (gas phase) molecules, interfaces and surfaces, thin films, membranes, proteins and nanomaterials (Srinivasan *et al.*, 2003; Zewail, 2006; Lobastov *et al.*, 2005; Chen *et al.*, 2006; Lobastov *et al.*, 2007; Shorokhov & Zewail, 2008; Chergui & Zewail, 2009). This is due to the high scattering cross section of electrons with matter, which is five to six orders of magnitude larger than that of X-rays (Henderson, 1995).

Most of chemistry and biology occur in condensed phases and, in particular, liquids. It is thus important to probe the chemical and biochemical dynamics in this environment. Furthermore, molecular (geometric) structure changes are triggered and/or accompanied by electronic structure changes, either under excitation by light or in the presence of a reactant. Ideally, one would like not only to probe the *molecular structure* changes in real time, but also to identify the *electronic structure* changes underlying them. In recent years, time-resolved X-ray absorption spectroscopy (XAS) has emerged as an ideal tool for the study of structural dynamics in

liquids (Chen, 2004; Bressler & Chergui, 2004, 2009; Bressler *et al.*, 2008; Chergui & Zewail, 2009).

1.1. X-ray absorption spectroscopy

X-ray absorption spectra are characterized by absorption edges, which are element specific and reflect the excitation of core electrons to the ionization threshold (Koningsberger & Prins, 1988; Stöhr, 1992; Rehr & Albers, 2000). An X-ray absorption spectrum consists of bound–bound transitions (below the ionization potential, IP, of the inner-shell electron), followed by the absorption edge jump itself. Right above the absorption edge one observes a complicated modulation of the absorption cross section owing to multiple scattering of the ionized photoelectron by its nearest neighbors in the molecule. This spectral range is called the XANES region (X-ray absorption near-edge structure) and it contains rich information about both the electronic (below the IP) and the geometric structure (above the IP), including bond angles and distances.

From ~ 50 eV above the IP to higher energies mainly single scattering events dominate, which result in a weak oscillatory modulation of the absorption cross section. This region is called the EXAFS region (extended X-ray absorption fine structure). It delivers precise information about the internuclear distance of the nearest neighbors from the absorbing central atom. Thus, one can obtain in one single spectrum simultaneous information about the valence electronic structure and about the nuclear arrangement of the atoms in the molecular system.

More specifically, the type of information that can be extracted from XANES and EXAFS are the following:

(i) The bound–bound XANES features are due to transitions from core orbitals to valence ones, and the latter are involved in chemical bonding and/or are transformed under vis–UV light excitation. Thus, one can investigate the occupancy of valence orbitals, the oxidation state of the system, the occurrence of charge-transfer processes, orbital delocalization, bonding and backbonding contributions *etc.* (Stöhr, 1992; de Groot, 2001; De Groot & Kotani, 2008) and their changes in the course of a chemical, biochemical or physical transformation.

(ii) Above ionization XANES multiple scattering resonances (also called shape resonances in molecular physics; Stöhr, 1992) can deliver information about bond distances and angles, as well as coordination numbers (Bianconi, 1988; Natoli *et al.*, 2003; Benfatto *et al.*, 2003; Benfatto & Della Longa, 2001).

(iii) The single scattering EXAFS region delivers information about bond distances and coordination numbers of the nearest neighbors around the absorbing atom. The structural analysis of EXAFS is much simpler than that of XANES, which is the reason why EXAFS is more commonly used in static studies of molecular structure, even though the EXAFS modulations are typically less than 10% of the edge jump.

Therefore XAS (XANES and EXAFS) offers the following advantages:

(i) It is atom selective.

(ii) It can detect species that are spectroscopically silent in the optical domain.

(iii) It can be implemented in any phase of matter (gas, liquid, solid) and in biological systems.

(iv) It delivers information about both the electronic and the geometric structure of the system under study.

(v) The information about geometric changes is local (*i.e.* one to three shells of neighbors around the species of interest), but this is not a problem since ultrashort timescales correspond to ultrashort distance changes.

These advantages are of particular interest in the study of molecular and biomolecular systems since most of natural and preparative chemistry as well as all of biology occur in the liquid phase. In the past ten years, time-resolved XAS has matured to a routine method on the picosecond timescale (Chen, 2001, 2004; Bressler & Chergui, 2004; Gawelda, Pham, van der Veen *et al.*, 2007; Bressler *et al.*, 2008; Chergui & Zewail, 2009), while the femtosecond time resolution has just been achieved (Bressler *et al.*, 2009), opening exciting perspectives for ultrafast structural dynamics of chemical and biological systems in liquids. Here we review these developments and discuss the future prospects that open up.

2. The methodology

In order to exploit time-resolved X-ray absorption spectroscopy for a wide range of photoinduced ultrafast processes in various environments, the X-ray source should fulfil a number of requirements:

(i) Continuum radiation covering the range from soft to hard X-ray energies.

(ii) Ultrashort pulses.

(iii) High photon fluxes.

(iv) High shot-to-shot, as well as long-term stability.

(v) Synchronization to an external light source (*e.g.* a pump laser).

The only X-ray sources that approach these requirements are third-generation synchrotron storage rings, albeit at the cost of a lower temporal resolution (tens of ps). However, the sub-ps range is now also possible at synchrotrons following the implementation of the so-called slicing scheme (Zholents & Zolotorev, 1996; Schoenlein *et al.*, 2000; Khan *et al.*, 2006; Beaud *et al.*, 2007), although at the cost of a largely reduced photon flux.

2.1. Data acquisition

The development and methodology of time-resolved XAS studies have been described by Bressler *et al.* (2001, 2002, 2008), Saes, Gawelda *et al.* (2003), Saes *et al.* (2004), Bressler & Chergui (2004) and Gawelda *et al.* (2005). The now established approach was implemented by the Lausanne group. It is based on recording the transient (difference) absorption on a shot-to-shot basis. Briefly, monochromatic X-rays are focused to *ca* 50 µm diameter onto the sample with a pair of KirkPatrick–Baez mirrors. X-ray signals are detected with four large-area

avalanche photodiodes (APDs), one each for transmission (I_1) and for the incident signal (I_0) scattered off a thin Cr foil, and two fluorescence APDs (I_{F1}, I_{F2}) for X-ray fluorescence from the sample. The sample consists of a free-flowing liquid jet, which is excited by ultrashort pulses from an amplified femtosecond laser system. Spatial overlap including a measurement of the spot sizes on the sample between both laser and X-ray beams is set *via* steering the laser beam onto the X-ray spot on the sample, monitored with an imaging CCD camera.

We exploit a special electron bunch-filling pattern at the Swiss Light Source (SLS) for recording laser-pump X-ray probe spectra (Fig. 1). The SLS storage ring consists of 480 so-called buckets, each separated by 2 ns, in which 390 are filled (a filled bucket is also called an electron bunch) with approximately 6×10^9 electrons, while in the subsequent 180 ns dark section a single densely packed (with up to five times more charge) hybrid electron bunch is placed. The X-ray pulse emitted from this electron bunch is used to probe the photoinduced changes of the X-ray absorption within the sample. The amplified laser system for photoexcitation runs at 1 kHz repetition rate, and is synchronized to the round trip frequency of the electron bunch (T = 960 ns), thus ensuring a constant time delay between the laser and selected probing X-ray pulses. A gated integrator delivers a sequence of output signals proportional to the input signal integrated over a fixed time window (Fig. 1). These signals are recorded with an analogue-to-digital converter card, triggered at 4 kHz, in order to provide a sequence of the X-ray signals when the laser is on and off, but also for recording the electronic

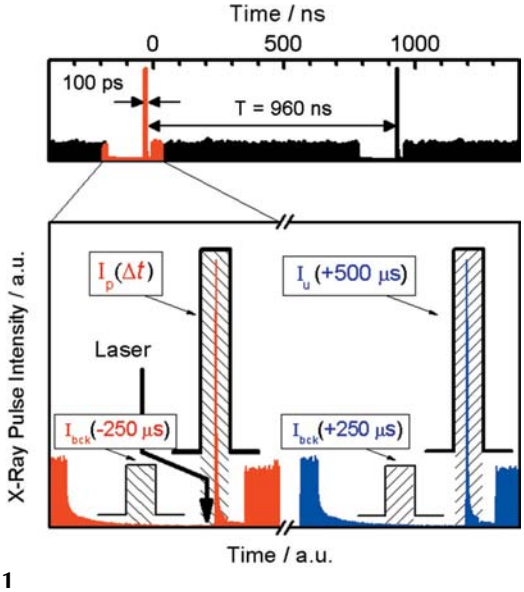

Figure 1
Top: typical bunch-filling pattern at the Swiss Light Source. Trains of 390 electron bunches with 2 ns spacing are followed by a 180 ns-long empty section, in which a densely packed electron bunch (pulse width 100 ps) is placed 30 ns before the start of the bunch train. Bottom: data-acquisition scheme. A gated integrator sequentially measures the X-ray intensity at the chosen time delay Δt, a background signal *ca* 250 μs earlier and later, and the X-ray signal of the unexcited sample after 500 μs (each within the indicated shaded time windows). This acquisition scheme is repeated several thousand times per data point.

background signal with no X-rays present. First, the X-ray signal at time Δt after laser excitation is measured (I_p), then a background signal without X-rays is recorded after *ca* 250 μs [I_{bck} (250 μs)], which enables post-correcting baseline drifts in the gated integrator, and finally, after 0.5 ms, the X-ray signal from a fresh sample without laser excitation is recorded (I_u) followed by a baseline correction measurement [I_{bck} (500 μs + 250 μs), not shown in the figure; Gawelda *et al.*, 2005; Gawelda, Pham, van der Veen *et al.*, 2007]. The pump–probe signal in transmission is defined as the transient absorption T_{tr} of the photoexcited sample *via* Gawelda *et al.* (2005) and Gawelda, Pham, van der Veen *et al.* (2007),

$$T_{tr}(E, \Delta t) = 1n\left(\frac{I_{pum}}{I_{unp}}\right), \quad (1)$$

with $I_{pum} = I_p\ (\Delta t) - I_{bck}\ (\Delta t + 250\ \mu s)$ and $I_{unp} = I_u\ (500\ \mu s) - I_{bck}\ (500\ \mu s + 250\ \mu s)$ being both the baseline (I_{bck}) corrected photoexcited and unexcited X-ray signals, respectively (see Fig. 1). The X-ray signals were measured simultaneously in transmission and fluorescence yield modes, using the same data acquisition strategy for all detectors, as shown in Fig. 1. We define the transient signal in fluorescence mode T_{fl} *via*

$$T_{fl}(E, \Delta t) = \frac{I^{fl}_{pum} - I^{fl}_{unp}}{I_0}, \quad (2)$$

with I^{fl}_{pum}, I^{fl}_{unp} and I_0 being each baseline-corrected as described above in transmission mode. Likewise, normalization of the unpumped spectra to the incident flux yields the static XAFS of the sample.

This data acquisition scheme permits us to measure the corresponding signals for every single incident X-ray pulse, and for each data point (*e.g.* during an energy scan) a few thousand single X-ray pulse intensities are analyzed in order to store the average value and its standard deviation into the computer. We have repeatedly confirmed that this methodology delivers accuracies, which are very close to what is expected from the X-ray source flux, *i.e.* down to the shot-noise limit of the source (Gawelda *et al.*, 2005; Gawelda, Pham, van der Veen *et al.*, 2007).

In summary, our data acquisition scheme:

(i) Eliminates drifts due to the deterioration of the sample under laser and/or X-ray irradiation (for limited sample volumes), as well as drifts in X-ray flux.

(ii) Allows measurements at the shot noise of the X-ray source, implying that changes as low as 10^{-4} X-ray transmission changes can be recorded within a reasonable (typically 1 s) data-acquisition time.

This strategy has now been adopted at different synchrotron centers (Khalil *et al.*, 2006; Chen *et al.*, 2007).

2.2. Data treatment and structural determination

A crucial point in all time-resolved X-ray studies is the extraction of the excited-state spectrum from the transient (difference transmission with the above described scheme) spectra, which is a prerequisite for the structural analysis.

Naturally, this is strongly sensitive to the precise determination of the photoexcitation yield, and thus a lack thereof may induce errors in the structural determination (Bressler *et al.*, 2008). In the simple case of a mere two-level system, the analysis uses the XAS spectrum of the ground and (extracted) excited state. Several codes exist that fit both the XANES (Tyson *et al.*, 1989, 1992; Natoli *et al.*, 1986; Benfatto *et al.*, 2006; Zabinsky *et al.*, 1995; Ankudinov *et al.*, 1998, 2002; Rehr & Albers, 2000) and the EXAFS (Mustre *et al.*, 1990; Rehr & Albers, 2000) regions. However, quite frequently it is difficult, if not impossible, to extract the excited-state fractional population from comparative optical-only studies, because the ground-state bleach is often overlapped by excited-state absorption or stimulated emission. In addition, populations extracted from laser-only studies need to be convoluted with the much longer X-ray pulse width, giving rise to additional ambiguities.

An alternative approach was developed that fits the transient EXAFS spectrum in energy space directly (Gawelda *et al.*, 2009). A series of EXAFS spectra are simulated for a collection of possible excited-state structures from which the ground-state fit spectrum is subtracted to generate transient spectra. These are then compared with the experimental transient absorption spectrum using a least-squares statistical analysis to derive the structural change. This approach reduces the number of required parameters by cancellation in the differences. It can also deliver a unique solution for both the fractional population and the extracted excited-state structure, next to quantifying electronic information about possible energy shifts (Gawelda *et al.*, 2009). A similar approach was proposed for fitting difference XANES spectra (Benfatto *et al.*, 2006). It is however clear that one needs to have a preconceived idea of the input structures, which are based on knowledge of the system and its realistic deformation geometries, as for example in the case of bimetallic complexes (see §3.2).

As for the extraction of electronic structure information from the bound–bound XANES features, the charge-transfer ligand-field multiplet theory (Okada *et al.*, 1992; Thole *et al.*, 1985; De Groot, 2005; De Groot & Kotani, 2008) has proven very successful on a wide range of systems, both in molecular and condensed matter physics. The theory takes into account all Coulomb interactions as well as the spin–orbit coupling between the atomic orbitals, and treats the geometric environment of the absorbing atom through a ligand-field potential. It also introduces orbital mixing between the central atom and its ligands *via* charge transfer terms. This tool has now been extended to model excited-state XANES spectra (Gawelda *et al.*, 2006), but here also the comparison with experiment is critically dependent on a most accurate determination of the fraction of excited-state population (Bressler *et al.*, 2008).

3. Applications

The first time-resolved X-ray experiment used X-ray absorption spectroscopy (XAS) to probe the photoinduced changes in carboxymyoglobin in solution with microsecond resolution (Mills *et al.*, 1984). Later, Wilson and co-workers (Raksi *et al.*, 1996) used 1.5–3 ps X-ray pulses from a plasma source to probe the disappearance of a shape resonance at the *K*-edge of sulfur upon photodissociation of the SF_6 molecule in the gas phase. Chen and co-workers reported the first study of a molecular system in solution, investigating the photodissociation of ligands from [Ni(tpp)L_2] [Ni(tpp) = nickel(II) tetraphenylporphyrin and L = axial piperidine ligand, which was also the solvent in their study], and their recoordination with 14 ns resolution using synchrotron X-ray pulses. They addressed the issue as to whether the recoordination process is a concerted or a sequential (two-step recombination with [Ni(tpp)L] as an intermediate) process. They concluded that the process was concerted, which is not surprising on the timescale of their resolution, since bimolecular reactions occur on femtosecond to picosecond timescales (Zewail, 2000*b*).

3.1. Intramolecular charge transfer and electronic structure

Metal-based molecular complexes, such as metalloporphyrins, haems or chlorophylls, are heavily involved in photoinduced energy and electron transfer in photosynthesis, oxygen transportation (Gray & Winkler, 1996; Gray, 2001), and functional molecular devices (Juris *et al.*, 1988; Gratzel, 2001). Given that the visible absorption of these complexes is dominated by the metal-to-ligand charge-transfer (MLCT) band, there is an issue of both intramolecular and subsequent intermolecular (*i.e.* solvent) structural rearrangements owing to the electron transfer. The Lausanne group addressed these issues in a picosecond Ru $L_{2,3}$-edge XAS study of aqueous ruthenium(II)-tris-2,2′-bipyridine ($[Ru^{II}(bpy)_3]^{2+}$) (Saes, Bressler *et al.*, 2003; Gawelda *et al.*, 2006). In the predominantly octahedral field of the complex, the *d*-orbitals split into a lower t_{2g} orbital and an upper e_g orbital (Fig. 2). These are further split by the addition of the trigonal distortion and by the spin–orbit interaction. Fig. 3 shows the ground-state (*a*) and transient XAS (*b*) spectra, next to the extracted excited-

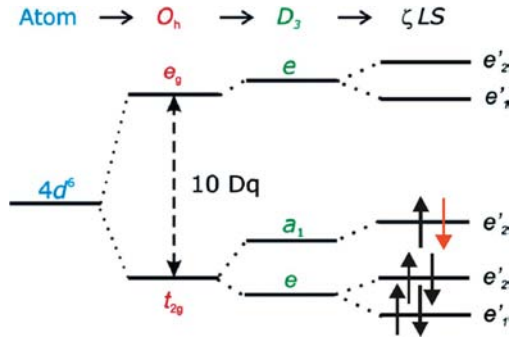

Figure 2
Energy-level scheme for $4d^6$ transition metal complexes such as $M(bpy)_3$, with M = Ru, Fe. The atomic 4*d* orbital splits into a sixfold degenerate t_{2g} and a fourfold degenerate e_g level in the octahedral field of the ligand (separated by 10 Dq). Trigonal distortion due to the D_3 symmetry of the complex partially lifts the degeneracy, which is further lifted into five levels by the 4*d* spin–orbit coupling. The electron occupancy of the ground state (completely filled in t_{2g} and empty for e_g) is indicated by the arrows, one (in red) is removed to the bpy ligand following photoexcitation of the MLCT states.

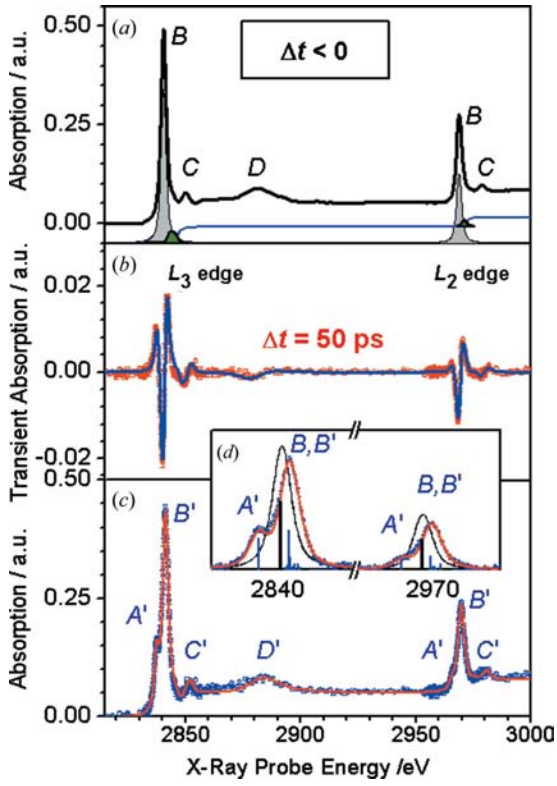

Figure 3
(*a*) $L_{2,3}$-edge XAS spectrum of aqueous $[Ru^{II}(bpy)_3]^{2+}$ in its ground state (thick black line) together with fits of its most prominent features (labeled), except for the two residual bands (green areas) near the ionization potential. The edge-step functions for IP for each state are also shown (blue line). See Gawelda *et al.* (2006) for details of the fit. (*b*) Transient absorption spectrum (open red circles with error bars) and a fit of this transient (blue line) using the ground-state spectrum and the (energy-shifted) decomposed bands shown in (*a*). (*c*) Reconstructed XAS of the ^{3}MLCT state (blue data points), together with a fit to the most prominent features. (*d*) The *A* (*A*′) and *B* (*B*′) features extracted from the spectrum after subtraction of the edge step and the higher-lying weak bound–bound absorptions shown in (*a*), and compared with multiplet calculations. The sticks (thick for the ground state and thin for the excited state) are the transitions which are broadened with the Gaussian and Lorentzian widths due to experimental resolution and lifetime width, to generate the solid (red) curves.

state XAS (*c*). In the ground state, all six 4*d* electrons are in the lower t_{2g} orbital while the e_g orbital is empty, and therefore only the *B* band [$2p \rightarrow 4d(e_g)$] appears. In the MLCT state, an electron is transferred to the bpy ligand, thus opening up a new transition [$2p \rightarrow 4d(t_{2g})$, feature *A*′]. In room-temperature aqueous solutions, the ^{3}MLCT state exhibits a measured lifetime of ~ 600 ns (Tarnovsky *et al.*, 2006). Also, the blue shift of the *B* feature reflects the change in oxidation state, in good agreement with previous experimental and theoretical work (De Groot *et al.*, 1994; Calzaferri & Rytz, 1995). The XANES region was analyzed by the ligand-field multiplet theory (Gawelda *et al.*, 2006) in very good agreement with the data (see Fig. 3*d*). From the change of ligand field splitting between ground and excited state, and using an electrostatic model that relates the octahedral ligand field splitting to the inverse fifth power of the metal–ligand distance (König & Watson, 1970), we could deduce an Fe—N bond contraction of ~ 0.02 Å in the excited state, which is confirmed below by the analysis of the EXAFS region.

The *D* (*D*′) feature in Fig. 3 is an EXAFS modulation. Its blue shift by 1 eV (after correcting for the shift of the ionization potential, see Gawelda *et al.*, 2006 for details) suggests a contraction of the Ru—N bond and the structural analysis (using *FEFF*8.20; Rehr & Albers, 2000) delivers a value of -0.037 ± 0.0135 Å (in fair agreement with the above-derived value), treating all Ru—N distances equally (*i.e.* in D_3 symmetry). This relatively weak bond contraction, despite a dramatic change in the electronic structure, results from steric effects because the three bpy ligands are already in a constrained geometry in the ground state. Our results were later confirmed by quantum chemical calculations of the ^{3}MLCT structure: Nozaki *et al.* (2006) reported a Ru—N bond contraction of 36 mÅ for the reduced bpy, and an elongation of 28 mÅ for the neutral bpy ligands in C_2 geometry, while the bond contraction was 7 mÅ in D_3 geometry. Alary *et al.* (2007) reported a bond elongation of 24 mÅ for one of the neutral bpys, no change for the second and a bond contraction of 13 mÅ for a reduced bpy under C_2 symmetry.

In another example of structural changes due to intramolecular electron-transfer processes, Chen and co-workers (Shaw *et al.*, 2007) investigated the structure of the MLCT states of cuprous diimine compounds by picosecond XAS. They observed the structural changes by EXAFS resulting from the photoexcited MLCT transition of $[Cu^I(dmp)_2]^+$ (dmp = 2,9-dimethyl-1,10-phenanthroline) that induces an electronic configuration change from Cu^I ($3d^{10}$) to Cu^{II} ($3d^9$). They found:

(i) A formally generated Cu^{II} excited-state center.

(ii) The inner-sphere reorganization changed the coordination number of the MLCT state from four to five in toluene, which is presumed to be non-coordinating.

(iii) The average Cu–ligand bond lengths increased in the MLCT state in toluene, but decreased in acetonitrile, reflecting the difference in the interactions of the copper with the fifth ligand.

These conclusions were further supported by simulations of the XANES part of the spectra (Smolentsev *et al.*, 2008).

3.2. Bond formation in bimetallic complexes

The triplet excited states of dinuclear d^8–d^8 platinum, rhodium and iridium complexes (bridged by various ligands) exhibit remarkable photophysical and photochemical properties, which are strongly determined by their structure (Vlcek, 2000). The unusually high photocatalytic activity of these complexes are a manifestation of the newly formed bond in the lowest excited singlet and triplet $^{1,3}A_{2u}$ states, owing to the promotion of an electron from the antibonding $d\sigma^*$ (d_{z^2}-derived) orbital to the bonding $p\sigma$ (p_z-derived) orbital, which should therefore lead to a contraction of the metal–metal bond (Fig. 4). The $[Pt_2(P_2O_5H_2)_4]^{4-}$ ion is among the most extensively studied molecules in the family of dinuclear metal complexes. In solutions, excitation into the first singlet state in the near-UV region around 370 nm leads to the formation of

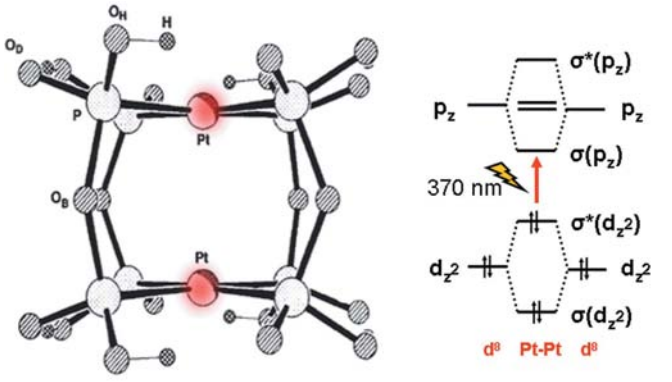

Figure 4
The $[Pt_2(P_2O_5H_2)_4]^{4-}$ molecule (left). Photoexcitation in the UV promotes an electron from the antibonding $d\sigma^*$ (d_{z^2}-derived) to the bonding $p\sigma$ (p_z-derived) orbitals, leading to the formation of the Pt—Pt bond and contraction of its distance in the excited state.

the long lived (∼1 µs) triplet state with unity quantum yield. Studies by resonance Raman spectroscopy, optical absorption and emission, and quasi-steady-state and time-resolved X-ray diffraction all pointed to a Pt—Pt bond shortening of around 0.2 Å, except for one significantly larger value obtained by EXAFS (see van der Veen *et al.*, 2009, for a review). Using picosecond EXAFS, van der Veen *et al.* (2009) resolved its structure. Fig. 5(*a*) shows the ground-state Pt L_3-edge XAS spectrum (black trace) as well as the transient spectrum, integrated from 0 to 150 ns to improve the signal-to-noise ratio. The inset shows the XANES region for the ground-state complex and its transient spectrum, wherein dramatic changes appear. In particular, a new absorption shows up at 11.574 keV below the absorption edge, which is due to the creation of a hole in the $5d\sigma^*$ orbital upon laser excitation, which can then be accessed from the $2p_{3/2}$ core orbital (L_3 edge). Clear changes are visible in the EXAFS region (Fig. 5*b*), reflecting structural modifications between the ground and excited triplet states.

From the transient EXAFS spectrum (Fig. 5*b*), the magnitude of the Pt—Pt bond contraction as well as, for the first time, changes affecting the Pt—P bonds were extracted. A collection of possible structural models (van der Veen *et al.*, 2009) were used to fit the data in energy space directly, according to the procedure (Gawelda *et al.*, 2009) described in §2.2, and the best fit is shown in Fig. 5(*b*). In particular, while the Pt—Pt bond contracts by 0.31 (5) Å, in very good agreement with the X-ray diffraction data, it was shown that Pt—P bonds slightly elongate (by ∼ 20 mÅ), in agreement with theoretical predictions (Novozhilova *et al.*, 2003). This work underscores the ability to retrieve details of the excited-state structure of a rather complex molecular system in liquid solution, owing to the high sensitivity of the experiment, coupled with a rigorous structural analysis based on fitting the transient EXAFS spectra directly in energy space (Gawelda *et al.*, 2009). Almost simultaneously to the work by van der Veen *et al.* (2009), Christensen *et al.* (2009) reported a picosecond X-ray scattering study of the same system, deriving a somewhat similar contraction of the Pt—Pt bond. It should be noted that their treatment departs from a ground-state structure determined by quantum chemical simulations.

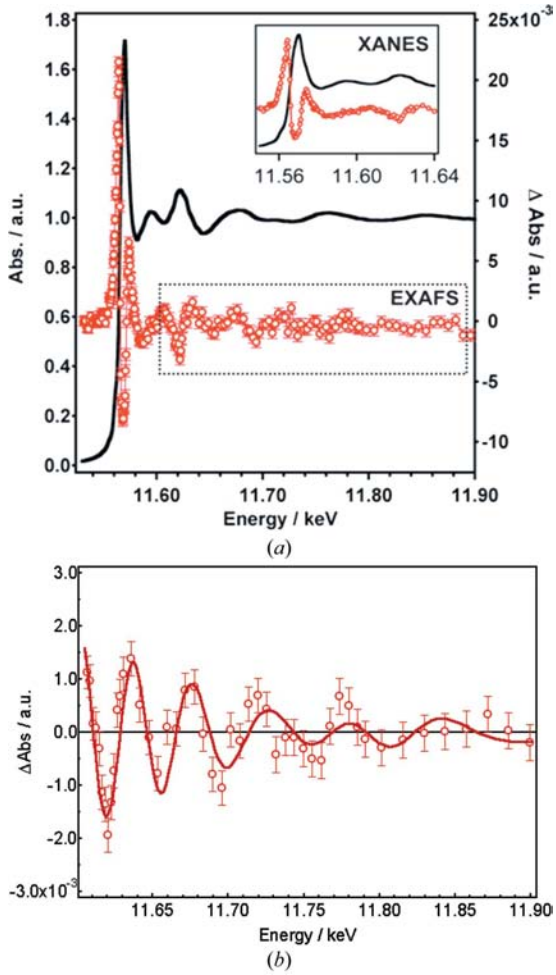

Figure 5
(*a*) Static Pt L_3 XAS spectrum of $[Pt_2(P_2O_5H_2)_4]^{4-}$ in solution (black line, left axis) and the transient (excited – unexcited) XAS spectrum (red circles, right axis, same units as left) integrated up to 150 ns after excitation. The inset zooms into the XANES region. (*b*) Transient EXAFS data and best fit (solid line) with the following parameters: a Pt—Pt contraction of 0.31 (5) Å, a Pt–ligand elongation of 0.010 (6) Å, zero energy shift and 7% excitation yield (see van der Veen *et al.*, 2008, 2009, for details).

3.3. Structure of high-spin states of Fe^{II}-based complexes

One of the fascinating features of Fe^{2+} or Fe^{3+} metal-based molecular complexes is their ability to change spin under temperature, pressure or light irradiation and they have therefore been named spin cross-over complexes (SCO; Hauser, 2004). In the predominantly octahedral field because of the ligands (Fig. 2), all electrons are in the lower t_{2g} subshell in the low-spin (LS) ground state, while transferring electrons to the e_g orbitals increases the spin state. Since the e_g orbitals derive from the $d_{x^2-y^2}$ and d_{z^2} orbitals, they are antibonding in sixfold coordinated complexes, which leads to a striking metal–ligand bond elongation in the high-spin (HS) state. A generic diagram of the energy curves of the various states of Fe^{II}-based complexes is shown in Fig. 6(*a*) as a

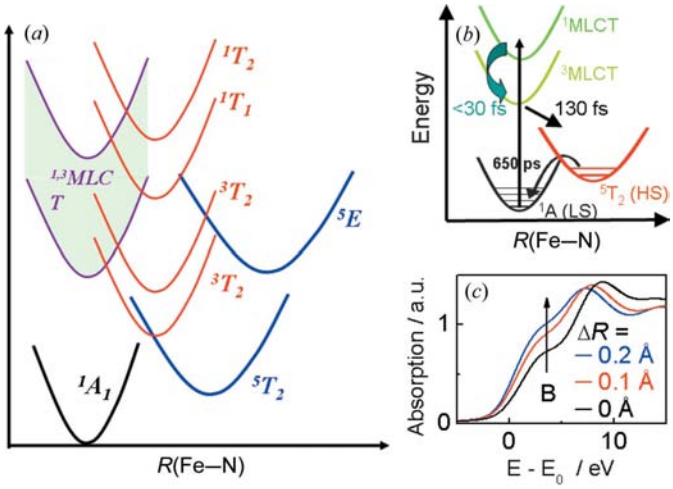

Figure 6
(*a*) Typical potential-energy curves of Fe^{II} complexes as a function of the Fe—N bond distance adapted from Ordejon *et al.* (2008). The manifold of MLCT states is shown as a shaded area. The metal-centered (MC) states are represented by their symmetry character (*A*, *T* and *E*) in the D_3 group. In the latter, the LS $^1A_1$ ground state has a completely filled $e^4a_1^2$ configuration (derived from the t_{2g}^6 subshell in O_h symmetry), while the antibonding *e* (e_g in the O_h symmetry) orbital is empty. Per electron promoted from the t_{2g} to the e_g subshell (for easier reading we will use hereon the O_h nomenclature), the metal–ligand bond length increases by as much as 0.1 Å (Ordejon *et al.*, 2008). For the series of $^{1,3}T(t_{2g}^5e_g)$ states, it is expected to be in between the ground and the high-spin $^5T_2$ ($t_{2g}^4e_g^2$) state. (*b*) Relaxation cascade as determined by ultrafast laser spectroscopy upon excitation of aqueous $[Fe(bpy)_3]^{2+}$ at 400 nm (Gawelda, Cannizzo *et al.*, 2007). The intermediate MC states are not shown as they are optically silent in the UV–vis and were therefore not observable. (*c*) Simulated XANES spectra for different Fe—N bond elongations from the ground-state equilibrium value of 1.97 Å, using the *MXAN* code (Benfatto *et al.*, 2003). The elongations correspond to the ground and the MLCT states (0 Å), the intermediate ligand field $^{1,3}T$ states (0.1 Å) and the ^5T state (0.2 Å). The horizontal axis is given as energy shift from the ionization potential.

function of the Fe—N bond length (Ordejon *et al.*, 2008). The MLCT states have almost the same equilibrium distance as the ground state, in agreement with Gawelda *et al.* (2006), the ligand field states $^{1,3}T$, ^5T and ^5E have their equilibrium distances elongated by ∼0.1 Å, ∼0.2 Å and ∼0.3 Å, respectively, relative to the ground-state bond distance. Light excitation into the singlet metal-to-ligand charge-transfer (^{1}MLCT) state or to the lower-lying ligand-field states leads to the population of the lowest quintet state $^5T_2$ with a quantum efficiency of 1 (Hauser, 2004). The lifetime of the latter varies by several orders of magnitude as a function of ligand and temperature (Hauser, 2004), with $[Fe(bpy)_3]^{2+}$ having the shortest-lived quintet state lifetime (650 ps) at room temperature. Structural studies by X-ray diffraction or X-ray absorption spectroscopy under quasi steady-state conditions pointed to a bond elongation of ∼0.2 Å of the Fe—N bond for Fe^{II}-based complexes with long-lived HS states (Guionneau *et al.*, 2004; Oyanagi *et al.*, 2004, 2006), but the question arose as to whether this applies to the shortest-lived HS state of $[Fe(bpy)_3]^{2+}$, as predicted by theory (Daku *et al.*, 2005).

This could only be tackled by XAS with picosecond resolution, and Gawelda, Pham, Benfatto *et al.* (2007) captured the structure of the quintet state after laser excitation using 70 ps hard X-ray pulses at the *K*-edge of iron. Fig. 7 shows the Fe *K*-edge XANES of the molecule in the ground state, the transient (difference) spectrum at 50 ps time delay and the XAS spectrum of the quintet state, as retrieved from the ground state and the difference spectra and from the photolysis yield determined in laser-only experiments (and convoluted to match the much longer X-ray probe width). The structural analysis of the excited state based on the transient XANES and EXAFS spectra was carried out in two ways:

(i) Fitting an excited-state EXAFS spectrum that was generated from the transient EXAFS spectrum, and the prior knowledge of the photolysis yield (Gawelda, Pham, Benfatto *et al.*, 2007).

(ii) Fitting directly the transient spectrum in energy space, as described in §§2.2 and 3.2 (Bressler *et al.*, 2008; Gawelda *et al.*, 2009).

These deliver the same Fe—N bond elongation, ΔR_{Fe-N} = 0.20 Å, but the precision increased considerably using the latter procedure (0.203 ± 0.008 Å). The fact that the bond elongation is nearly the same in the HS state of all Fe^{II}-based complexes (Guionneau *et al.*, 2004; Khalil *et al.*, 2006) shows that it is not the parameter that controls the quintet-state lifetime. Rather, the adiabatic energy and the coupling parameters between low- and high-spin states are the crucial parameters. Indeed, of all Fe^{II}-SCO complexes, $[Fe^{II}(bpy)_3]^{2+}$ has the highest lying quintet state.

Chen *et al.* (2007) also investigated the structure change of nickel tetramesitylporphyrin (Ni^{II}TMP) in an excited triplet state. They found that the nearly square-planar singlet ground state, which has an empty $3d_{x^2-y^2}$ orbital and a doubly occupied $3d_{z^2}$ orbital according to ligand field theory, undergoes an Ni—N bond elongation of 0.08 Å in the lowest triplet state, presumably owing to a configuration where the $3d_{x^2-y}$ and $3d_{z^2}$ orbitals are each singly occupied. The occupancy of the 3*d* orbitals was probed on the dipole-forbidden 1*s*–3*d* transitions

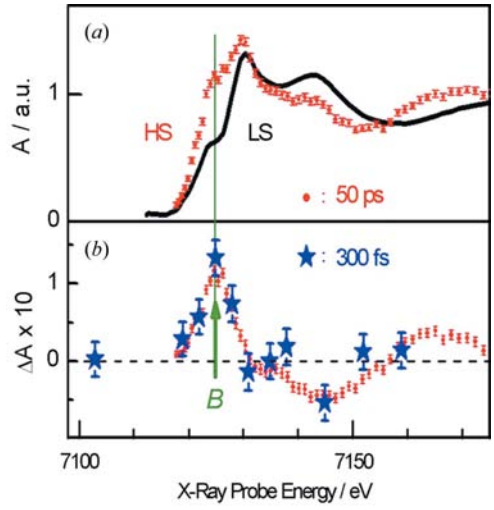

Figure 7
(*a*) XANES spectrum of the LS state of $[Fe^{II}(bpy)_3]^{2+}$ (black) and the HS state (red points). The latter is extracted from the difference spectrum (*b*) and the LS spectrum, based on the prior determination of the fraction of excited molecules. (*b*) Difference transient spectrum at 50 ps time delay (red points) and at 300 fs (blue stars) obtained with the slicing scheme.

in the pre-edge region of the *K*-edge spectrum, delivering a direct estimate of the ligand field in the T_1 state. This study stressed once more that a precise knowledge of the fractional population is critical (Della-Longa *et al.*, 2009).

3.4. Femtosecond probing of structural dynamics

The mechanism and relaxation pathways of the above photoinduced LS–HS conversion in Fe^{II} complexes have long been debated (Hauser, 2004; Monat & McCusker, 2000; Juban *et al.*, 2006). One of the reasons is that the intermediate $^{1,3}T$ state (Fig. 6*a*) is optically silent, while the HS quintet state has an absorption below 320 nm (McCusker *et al.*, 1996). The early time dynamics were identified by Gawelda *et al.* in laser-only studies (Gawelda, Cannizzo *et al.*, 2007), who found that departure from the ^{3}MLCT state occurs in $\sim$130 fs (Fig. 6*b*). The XANES spectrum of the ground state (Fig. 7) shows a shoulder (the *B* feature) on the edge, which is a multiple scattering feature (Briois *et al.*, 2001). Upon Fe—N bond elongation in the quintet state its intensity increases causing the significant peak at low energy in the transient spectrum (Fig. 7*b*). Simulations based on multiple scattering theories confirm the distance dependence of the *B* feature (Fig. 6*c*), which one can use to identify the various electronic states possibly involved in the relaxation cascade.

Using hard X-ray femtosecond pulses generated by the slicing scheme, Bressler *et al.* carried out an optical pump/X-ray probe experiment following the evolution of the *B* feature as a function of pump–probe delay. Fig. 8 displays the time scan obtained at the *B* feature (7.122 keV) showing that the signal stabilizes from about 300 fs up to the scan limit of 10 ps (see inset), which is evidence that the system is already in the quintet state. Further evidence is the energy scan at 300 fs, which reproduces the transient spectrum at 50 ps time resolution (Fig. 7*b*). The fit in Fig. 8 shows that the quintet state is reached in 150 ± 50 fs. This time corresponds to the decay of the ^{3}MLCT state, implying that the ultrafast spin conversion is a simple three-step ^{1}MLCT–^{3}MLCT–$^5T_2$ cascade that bypasses the intermediate $^{1,3}T$ states. The timescale of $\sim$150 fs corresponds to about two oscillations of the Fe—N stretch vibration (Tuchagues *et al.*, 2004), suggesting a nearly non-Born–Oppenheimer process. This experiment illustrates the power of ultrafast XAS to retrieve dynamical information difficult to obtain by laser-only experiments. It also shows how structural dynamics studies can identify the electronic relaxation pathways of complex molecules, while so far the opposite was common practice. Further visible pump/UV probe transient experiments of the quintet state identified its vibrational relaxation dynamics (Consani *et al.*, 2009), thus providing a complete picture of the photocycle of aqueous $[Fe^{II}(bpy)_3]^{2+}$. A full description of the combined optical and X-ray studies on this system is given in a recent review (Cannizzo *et al.*, 2010).

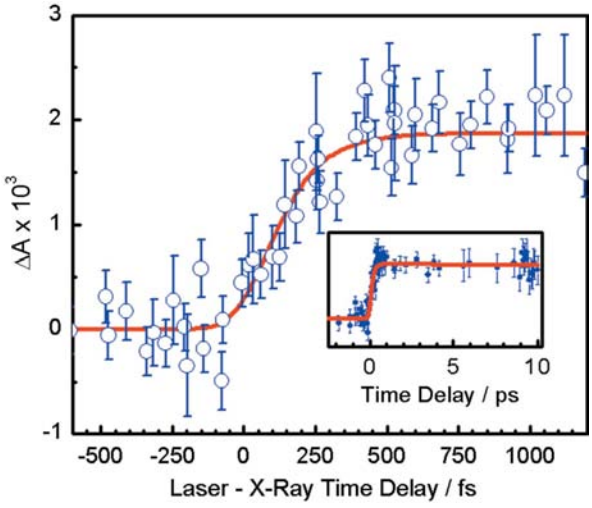

Figure 8
Time scan of the signal (blue points) at the *B* feature (Fig. 6*c*), as a function of laser pump/X-ray probe time delay after excitation of aqueous $[Fe^{II}(bpy)_3]^{2+}$ at 400 nm. The inset shows a long time scan up to 10 ps time delay. The red trace is the simulated signal assuming a simple four-step kinetic model $^1A_1 \rightarrow {}^1$MLCT $\rightarrow {}^3$MLCT $\rightarrow {}^5T$ to describe the spin conversion process. The amplitude of the signal corresponds to the expected absorption increase for an elongation of 0.2 Å for the Fe—N distance ΔR between the LS and HS states (see Fig. 6*c*).

4. Conclusions and outlook

The above review presents recent advances in picosecond and femtosecond hard X-ray absorption spectroscopy. Picosecond can now can be considered as a routine technique that can be applied to a large class of molecular systems in solution, but also to the probing of atomic ions in solutions, as recently demonstrated in the case of aqueous iodide (Pham *et al.*, 2007) and bromide (Elles *et al.*, 2008). These studies have been limited to systems containing heavy atoms, since the solvent absorption is weak in the hard X-ray range. Furthermore, they have been limited to chemical systems, even though the desire to carry out studies on biological systems in physiological media has been stressed in the introduction to the technique and, as already mentioned, the first time-resolved XAS was carried out on biological systems (Mills *et al.*, 1984). Such studies are still commonly being carried out with milli- to microsecond resolution (Chen *et al.*, 1999; Wang *et al.*, 2005; Haumann, Liebisch *et al.*, 2005; Haumann, Muller *et al.*, 2005; Arcovito *et al.*, 2005; Oyanagi *et al.*, 2004, 2006). One of the aims of current studies is to extend them to higher temporal resolutions.

Several exciting prospects are on the way thanks to recent developments in the implementation of methodologies:

(i) All the above experiments were carried out using a pump laser at 1 kHz repetition rate, while the storage ring operates at MHz repetition rates. This implies that typically 10^3 X-ray photons remain unused. The implementation of high-repetition-rate lasers (running at hundreds of kHz) that match an integer fraction of the storage ring repetition rate, combined with microfocusing of the X-ray and laser beams (this is possible at several synchrotron beamlines), should allow a significant increase of signal-to-noise, and, therefore, the possibility of reducing the data acquisition times and of working at much lower dilutions than in the present situation

(tens of millimolars), thus approaching the concentration of biological samples.

(ii) Now that the femtosecond resolution capability of the slicing scheme has been demonstrated (Bressler *et al.*, 2009), more studies should be possible and are already under way (Pham *et al.*, 2010).

(iii) Extension of time-resolved XAS to the soft X-ray regime (which we predicted in Bressler & Chergui, 2004; Bressler *et al.*, 2008) offers very exciting new advantages: (i) most *L*-edge spectra of transition metals lie in the 200–2000 eV region; (ii) it allows the probing of light elements such as C, N, O, S, P *etc.*, which are very important to biology. The limitation of soft X-ray spectroscopies of high-vapor-pressure samples has recently been overcome thanks to the use of high-speed liquid jets in vacuum chambers or of cells equipped with soft X-ray transparent windows (silicon nitride windows; Winter & Faubel, 2006). These approaches have already yielded a wealth of new results on chemical systems (Aziz *et al.*, 2007; Aziz, Eisebitt *et al.*, 2008; Aziz, Ottoson, Eisebitt *et al.*, 2008; Aziz, Ottoson, Faubel *et al.*, 2008), and even biological systems (Aziz *et al.*, 2009; Bergmann *et al.*, 2010). Recently these techniques have entered the picosecond time domain, by probing transient changes of liquid water heated by an ultrashort infrared laser pulse (Huse *et al.*, 2009; Gavrila *et al.*, 2009) and of photoexcited solvated molecules (Huse & Schoenlein, 2009).

(iv) Core-level spectroscopies, such as Auger spectroscopy, X-ray emission spectroscopy (XES), UV photoelectron spectroscopy (UPS) and X-ray photoelectron spectroscopy (XPS) are very well established techniques to probe the *electronic* structure of molecular systems, and have also been implemented in the static mode on high-vapor-pressure liquids (Winter & Faubel, 2006). Their extension into the time domain is also underway, and recent femtosecond UPS results were reported on various species in solution using a high harmonic VUV source (Link *et al.*, 2009), while the first picosecond XES on $[Fe^{II}(bpy)_3]^{2+}$ have been obtained (Vanko *et al.*, 2010).

In conclusion, the prospects are bright for ultrafast X-ray absorption spectroscopy. While the upcoming X-ray free electron lasers offer a dramatic increase in flux and time resolution, problems due to tunability and stability need to be solved to make them usable for X-ray absorption studies. Therefore, synchrotrons remain the most reliable sources of X-ray photons for such applications. Combined with the slicing scheme or the use of ultrafast X-ray streak cameras, they will provide the sub-picosecond time resolution along with an unsurpassed degree of stability and for broad tunability.

Deep thanks to my co-workers who have contributed to the various studies presented here: Ch. Bressler, C. Milne, M. Kaiser, W. Gawelda, V.-T. Pham, A. ElNahhas, R. M. van der Veen and F. van Mourik. We also acknowledge the great collaboration with the team at the MicroXAS beamline of the Swiss Light Source (PSI, Villigen): S. Johnson, P. Beaud, D. Grolimund, C. N. Borca, G. Ingold and R. Abela. Many thanks to M. Benfatto (Rome) and A. Hauser (Geneva) for useful discussions and for samples.

References

Alary, F., Heully, J. L., Bijeire, L. & Vicendo, P. (2007). *Inorg. Chem.* **46**, 3154–3165.
Ankudinov, A. L., Bouldin, C. E., Rehr, J. J., Sims, J. & Hung, H. (2002). *Phys. Rev. B*, **65**, 104107.
Ankudinov, A. L., Ravel, B., Rehr, J. J. & Conradson, S. D. (1998). *Phys. Rev. B*, **58**, 7565–7576.
Arcovito, A., Lamb, D. C., Nienhaus, G. U., Hazemann, J. L., Benfatto, M. & Longa, S. D. (2005). *Biophys. J.* **88**, 2954–2964.
Aziz, E. F., Eisebitt, S., Eberhardt, W., Cwiklik, L. & Jungwirth, P. (2008). *J. Phys. Chem. B*, **112**, 1262–1266.
Aziz, E. F., Grasjo, J., Forsberg, J., Andersson, E., Soderstrom, J., Duda, L., Zhang, W. H., Yang, J. L., Eisebitt, S., Bergstrom, C., Luo, Y., Nordgren, J., Eberhardt, W. & Rubensson, J. E. (2007). *J. Phys. Chem. A*, **111**, 9662–9669.
Aziz, E. F., Ottosson, N., Bonhommeau, S., Bergmann, N., Eberhardt, W. & Chergui, M. (2009). *Phys. Rev. Lett.* **102**, 68103.
Aziz, E. F., Ottosson, N., Eisebitt, S., Eberhardt, W., Jagoda-Cwiklik, B., Vacha, R., Jungwirth, P. & Winter, B. (2008). *J. Phys. Chem. B*, **112**, 12567–12570.
Aziz, E. F., Ottosson, N., Faubel, M., Hertel, I. V. & Winter, B. (2008). *Nature (London)*, **455**, 89–91.
Bargheer, M., Zhavoronkov, N., Woerner, M. & Elsaesser, T. (2006). *ChemPhysChem*, **7**, 783–792.
Beaud, P., Johnson, S. L., Streun, A., Abela, R., Abramsohn, D., Grolimund, D., Krasniqi, F., Schmidt, T., Schlott, V. & Ingold, G. (2007). *Phys. Rev. Lett.* **99**, 174801.
Benfatto, M. & Della Longa, S. (2001). *J. Synchrotron Rad.* **8**, 1087–1094.
Benfatto, M., Della Longa, S., Hatada, K., Hayakawa, K., Gawelda, W., Bressler, C. & Chergui, M. (2006). *J. Phys. Chem. B*, **110**, 14035–14039.
Benfatto, M., Della Longa, S. & Natoli, C. R. (2003). *J. Synchrotron Rad.* **10**, 51–57.
BenNun, M., Cao, J. S. & Wilson, K. R. (1997). *J. Phys. Chem. A*, **101**, 8743–8761.
Bergmann, N., Bonhommeau, S., Greil, S. M., Lange, K. M., Eisebitt, S., de Groot, F. M. F., Chergui, M. & Aziz, E. F. (2010). *Phys. Chem. Chem. Phys.* Submitted.
Bergsma, J. P., Coladonato, M. H., Edelsten, P. M., Kahn, J. D., Wilson, K. R. & Fredkin, D. R. (1986). *J. Chem. Phys.* **84**, 6151–6160.
Bianconi, A. (1988). *XANES Spectroscopy, X-ray Absorption Principles, Applications, Techniques of EXAFS, SEXAFS and XANES*, edited by D. C. P. Koningsberger, pp. XII, 673. New York: Wiley.
Bressler, C., Abela, R. & Chergui, M. (2008). *Z. Kristallogr.* **223**, 307–321.
Bressler, C. & Chergui, M. (2004). *Chem. Rev.* **104**, 1781–1812.
Bressler, C. & Chergui, M. (2010). *Annu. Rev. Phys. Chem.* **61**, 263–282.
Bressler, C., Milne, C., Pham, V. T., ElNahhas, A., van der Veen, R. M., Gawelda, W., Johnson, S., Beaud, P., Grolimund, D., Kaiser, M., Borca, C. N., Ingold, G., Abela, R. & Chergui, M. (2009). *Science*, **323**, 489–492.
Bressler, C., Saes, M., Chergui, M., Abela, R. & Pattison, P. (2001). *Nucl. Instrum. Methods Phys. Res. A*, **467**, 1444–1446.
Bressler, C., Saes, M., Chergui, M., Grolimund, D., Abela, R. & Pattison, P. (2002). *J. Chem. Phys.* **116**, 2955–2966.
Briois, V., Sainctavit, P., Long, G. J. & Grandjean, F. (2001). *Inorg. Chem.* **40**, 912–918.
Calzaferri, G. & Rytz, R. (1995). *J. Phys. Chem.* **99**, 12141–12150.
Cannizzo, A., Milne, C., Van Mourik, F., Bressler, C. & Chergui, M. (2010). *Coordin. Chem. Rev.* In the press.
Cao, J. S. & Wilson, K. R. (1998). *J. Phys. Chem. A*, **102**, 9523–9530.

Cavalleri, A. & Schoenlein, R. W. (2004). *Top. Appl. Phys.*, **92**, 309–337.
Chen, L. X. (2001). *J. Electron Spectrosc.* **119**, 161–174.
Chen, L. X. (2004). *Angew. Chem. Int. Ed.* **43**, 2886–2905.
Chen, L. X., Lee, P. L., Gosztola, D., Svec, W. A., Montano, P. A. & Wasielewski, M. R. (1999). *J. Phys. Chem. B*, **103**, 3270–3274.
Chen, L. X., Zhang, X. Y., Wasinger, E. C., Attenkofer, K., Jennings, G., Muresan, A. Z. & Lindsey, J. S. (2007). *J. Am. Chem. Soc.* **129**, 9616.
Chen, S., Seidel, M. T. & Zewail, A. H. (2006). *Angew. Chem. Int. Ed.* **45**, 5154–5158.
Chergui, M. & Zewail, A. H. (2009). *ChemPhysChem*, **10**, 28–43.
Christensen, M., Haldrup, K., Bechgaard, K., Feidenhans'l, R., Kong, Q. Y., Cammarata, M., Lo Russo, M., Wulff, M., Harrit, N. & Nielsen, M. M. (2009). *J. Am. Chem. Soc.* **131**, 502–508.
Collet, E., Boillot, M.-L., Hebert, J., Moisan, N., Servol, M., Lorenc, M., Toupet, L., Buron-Le Cointe, M., Tissot, A. & Sainton, J. (2009). *Acta Cryst.* B**65**, 474–480.
Collet, E., Cointe, M. B. L., Lorenc, M. & Cailleau, H. (2008). *Z. Kristallogr.* **223**, 272–282.
Consani, C., Prémont-Schwarz, M., El Nahhas, A., Bressler, C., van Mourik, F., Cannizzo, A. & Chergui, M. (2009). *Angew. Chem. Int. Ed.* **48**, 7184–7187.
Daku, L. M. L., Vargas, A., Hauser, A., Fouqueau, A. & Casida, M. E. (2005). *ChemPhysChem*, **6**, 1393–1410.
De Groot, F. (2001). *Chem. Rev.* **101**, 1779–1808.
De Groot, F. (2005). *Coord. Chem. Rev.* **249**, 31–63.
De Groot, F. & Kotani, A. (2008). *Core Level Spectroscopy of Solids*. New York: Taylor and Francis.
De Groot, F. M. F., Hu, Z. W., Lopez, M. F., Kaindl, G., Guillot, F. & Tronc, M. (1994). *J. Chem. Phys.* **101**, 6570–6576.
Della-Longa, S., Chen, L. X., Frank, P., Hayakawa, K., Hatada, K. & Benfatto, M. (2009). *Inorg. Chem.* **48**, 3934–3942.
Elles, C. G., Shkrob, I. A., Crowell, R. A., Arms, D. A. & Landahl, E. C. (2008). *J. Chem. Phys.* **128**, 061102.
Gaffney, K. J. & Chapman, H. N. (2007). *Science*, **316**, 1444–1448.
Gavrila, G., Godehusen, K., Weniger, C., Nibbering, E. T. J., Elsaesser, T., Eberhardt, W. & Wernet, P. (2009). *Appl. Phys. A*, **96**, 11–18.
Gawelda, W., Bressler, C., Saes, M., Kaiser, M., Tarnovsky, A., Grolimund, D., Johnson, S. L., Abela, R. & Chergui, M. (2005). *Phys. Scr.* T**115**, 102.
Gawelda, W., Cannizzo, A., Pham, V. T., van Mourik, F., Bressler, C. & Chergui, M. (2007). *J. Am. Chem. Soc.* **129**, 8199–8206.
Gawelda, W., Johnson, M., De Groot, F. M. F., Abela, R., Bressler, C. & Chergui, M. (2006). *J. Am. Chem. Soc.* **128**, 5001–5009.
Gawelda, W., Pham, V. T., Benfatto, M., Zaushytsin, Y., Kaiser, M., Grolimund, D., Johnson, S., Abela, R., Bressler, C. & Chergui, M. (2007). *Phys. Rev. Lett.* **98**, 057401.
Gawelda, W., Pham, V. T., El Nahhas, A., Kaiser, M., Zaushytsin, Y., Johnson, S., Grolimund, D., Abela, R., Hauser, A., Bressler, C. & Chergui, M. (2007). *AIP Conf. Proc.* **882**, 31.
Gawelda, W., Pham, V. T., van der Veen, R. M., Grolimund, D., Abela, R., Chergui, M. & Bressler, C. (2009). *J. Chem. Phys.* **130**, 124520.
Gratzel, M. (2001). *Nature (London)*, **414**, 338–344.
Gray, H. B. (2001). *Electron Transfer in Metalloproteins, Electron Transfer in Chemistry*, edited by V. Balzani. Weinheim: Wiley-VCH.
Gray, H. B. & Winkler, J. R. (1996). *Ann. Rev. Biochem.* **65**, 537–561.
Guionneau, P., Marchivie, M., Bravic, G., Letard, J. F. & Chasseau, D. (2004). *Top. Curr. Chem.* **234**, 97–128.
Haumann, M., Liebisch, P., Muller, C., Barra, M., Grabolle, M. & Dau, H. (2005). *Science*, **310**, 1019–1021.
Haumann, M., Müller, C., Liebisch, P., Neisius, T. & Dau, H. (2005). *J. Synchrotron Rad.* **12**, 35–44.
Hauser, A. (2004). *Spin Crossover in Transition Metal Compounds*, *Topics in Current Chemistry*, Vol. 234, pp. 155–198. Berlin: Springer.
Henderson, R. (1995). *Q. Rev. Biophys.* **28**, 171.
Huse, N. & Schoenlein, R. (2009). Personal communication.
Huse, N., Wen, H. D., Nordlund, D., Szilagyi, E., Daranciang, D., Miller, T. A., Nilsson, A., Schoenlein, R. W. & Lindenberg, A. M. (2009). *Phys. Chem.* **11**, 3951–3957.
Ihee, H. (2009). *Acc. Chem. Res.* **42**, 356–366.
Ihee, H., Rajagopal, S., Srajer, V., Pahl, R., Anderson, S., Schmidt, M., Schotte, F., Anfinrud, P. A., Wulff, M. & Moffat, K. (2005). *Proc. Natl. Acad. Sci. USA*, **102**, 7145–7150.
Ingold, G., Abela, R., Beaud, P., Johnson, S. L. & Staub, U. (2008). *Z. Kristallogr.* **223**, 292–306.
Johnson, S. L., Beaud, P., Milne, C. J., Krasniqi, F. S., Zijlstra, E. S., Garcia, M. E., Kaiser, M., Grolimund, D., Abela, R. & Ingold, G. (2008). *Phys. Rev. Lett.* **100**, 155501.
Juban, E. A., Smeigh, A. L., Monat, J. E. & McCusker, J. K. (2006). *Coord. Chem. Rev.* **250**, 1783–1791.
Juris, A., Balzani, V., Barigelletti, F., Campagna, S., Belser, P. & Vonzelewsky, A. (1988). *Coord. Chem. Rev.* **84**, 85–277.
Khalil, M., Marcus, M. A., Smeigh, A. L., McCusker, J. K., Chong, H. H. W. & Schoenlein, R. W. (2006). *J. Phys. Chem. A*, **110**, 38–44.
Khan, S., Holldack, K., Kachel, T., Mitzner, R. & Quast, T. (2006). *Phys. Rev. Lett.* **97**, 074801.
Kim, T. K., Lee, J. H., Wulff, M., Kong, Q. Y. & Ihee, H. (2009). *ChemPhysChem*, **10**, 1958–1980.
König, E. & Watson, K. J. (1970). *Chem. Phys. Lett.* **6**, 457–459.
Koningsberger, D. C. & Prins, R. (1988). *X-ray Absorption: Principles, Applications, Techniques of EXAFS, SEXAFS and XANES*. New York: Wiley.
Link, O., Lugovoy, E., Siefermann, K., Liu, Y., Faubel, M. & Abel, B. (2009). *Appl. Phys. A*, **96**, 117–135.
Lobastov, V. A., Srinivasan, R. & Zewail, A. H. (2005). *Proc. Natl. Acad. Sci. USA*, **102**, 7069–7073.
Lobastov, V. A., Weissenrieder, J., Tang, J. & Zewail, A. H. (2007). *Nano Lett.* **7**, 2552–2558.
Lorenc, M., Hebert, J., Moisan, N., Trzop, E., Servol, M., Buron-Le Cointe, M., Cailleau, H., Boillot, M. L., Pontecorvo, E., Wulff, M., Koshihara, S. & Collet, E. (2009). *Phys. Rev. Lett.* **103**, 028301.
McCusker, J. K., Rheingold, A. L. & Hendrickson, D. N. (1996). *Inorg. Chem.* **35**, 2100–2112.
Mills, D. M., Lewis, A., Harootunian, A., Huang, J. & Smith, B. (1984). *Science*, **223**, 811–813.
Monat, J. E. & McCusker, J. K. (2000). *J. Am. Chem. Soc.* **122**, 4092–4097.
Mustre, J., Yacoby, Y., Stern, E. A. & Rehr, J. J. (1990). *Phys. Rev. B*, **42**, 10843–10851.
Natoli, C. R., Benfatto, M., Della Longa, S. & Hatada, K. (2003). *J. Synchrotron Rad.* **10**, 26–42.
Natoli, C. R., Benfatto, M. & Doniach, S. (1986). *Phys. Rev. A*, **34**, 4682–4694.
Novozhilova, I. V., Volkov, A. V. & Coppens, P. (2003). *J. Am. Chem. Soc.* **125**, 1079–1087.
Nozaki, K., Takamori, K., Nakatsugawa, Y. & Ohno, T. (2006). *Inorg. Chem.* **45**, 6161–6178.
Okada, K., Kotani, A. & Thole, B. T. (1992). *J. Electron Spectrosc.* **58**, 325–343.
Ordejon, B., De Graaf, C. & Sousa, C. (2008). *J. Am. Chem. Soc.* **130**, 13961–13968.
Oyanagi, H., Tayagaki, T. & Tanaka, K. (2004). *J. Phys. Chem. Solids*, **65**, 1485–1489.
Oyanagi, H., Tayagaki, T. & Tanaka, K. (2006). *J. Lumin.* **119**, 361–369.
Perman, B., Srajer, V., Ren, Z., Teng, T. Y., Pradervand, C., Ursby, T., Bourgeois, D., Schotte, F., Wulff, M., Kort, R., Hellingwerf, K. & Moffat, K. (1998). *Science*, **279**, 1946–1950.
Pham, V. T., Gawelda, W., Zaushytsin, Y., Kaiser, M., Grolimund, D., Johnson, S., Abela, R., Bressler, C. & Chergui, M. (2007). *J. Am. Chem. Soc.* **129**, 1530–1531.

Pham, V. T., Milne, C., Bressler, C. & Chergui, M. (2010). In preparation.
Raksi, F., Wilson, K. R., Jiang, Z. M., Ikhlef, A., Cote, C. Y. & Kieffer, J. C. (1996). *J. Chem. Phys.* **104**, 6066–6069.
Rehr, J. J. & Albers, R. C. (2000). *Rev. Mod. Phys.* **72**, 621–654.
Ren, Z., Perman, B., Srajer, V., Teng, T. Y., Pradervand, C., Bourgeois, D., Schotte, F., Ursby, T., Kort, R., Wulff, M. & Moffat, K. (2001). *Biochemistry*, **40**, 13788–13801.
Rose-Petruck, C., Jimenez, R., Guo, T., Cavalleri, A., Siders, C. W., Raksi, F., Squier, J. A., Walker, B. C., Wilson, K. R. & Barty, C. P. J. (1999). *Nature (London)*, **398**, 310–312.
Saes, M., Bressler, C., Abela, R., Grolimund, D., Johnson, S. L., Heimann, P. A. & Chergui, M. (2003). *Phys. Rev. Lett.* **90**, 047403.
Saes, M., Bressler, C., van Mourik, F., Gawelda, W., Kaiser, M., Chergui, M., Bressler, C., Grolimund, D., Abela, R., Glover, T. E., Heimann, P. A., Schoenlein, R. W., Johnson, S. L., Lindenberg, A. M. & Falcone, R. W. (2004). *Rev. Sci. Instrum.* **75**, 24–30.
Saes, M., Gawelda, W., Kaiser, M., Tarnovsky, A., Bressler, C., Chergui, M., Johnson, S. L., Grolimund, D. & Abela, R. (2003). *Synchrotron Radiat. News*, **16**, 12.
Schmizing, C. V., Bargheer, M., Woerner, M. & Elsaesser, T. (2008). *Z. Kristallogr.* **223**, 283–291.
Schmizing, C. V. K., Bargheer, M., Kiel, M., Zhavoronkov, N., Woerner, M., Elsaesser, T., Vrejoiu, I., Hesse, D. & Alexe, M. (2007). *Phys. Rev. Lett.* **98**, 248301.
Schoenlein, R. W., Chattopadhyay, S., Chong, H. H. W., Glover, T. E., Heimann, P. A., Shank, C. V., Zholents, A. A. & Zolotorev, M. S. (2000). *Science*, **287**, 2237–2240.
Schotte, F., Anfinrud, P. A., Hummer, G. & Wulff, M. (2004). *Biophys. J.* **86**, 525A.
Schotte, F., Lim, M. H., Jackson, T. A., Smirnov, A. V., Soman, J., Olson, J. S., Phillips, G. N., Wulff, M. & Anfinrud, P. A. (2003). *Science*, **300**, 1944–1947.
Shaw, G. B., Grant, C. D., Shirota, H., Castner, E. W., Meyer, G. J. & Chen, L. X. (2007). *J. Am. Chem. Soc.* **129**, 2147–2160.
Shorokhov, D. & Zewail, A. H. (2008). *Phys. Chem.* **10**, 2879–2893.
Siders, C. W., Cavalleri, A., Sokolowski-Tinten, K., Toth, C., Guo, T., Kammler, M., von Hoegen, M. H., Wilson, K. R., von der Linde, D. & Barty, C. P. J. (1999). *Science*, **286**, 1340–1342.
Smolentsev, G., Soldatov, A. V. & Chen, L. X. (2008). *J. Phys. Chem. A*, **112**, 5363–5367.
Srajer, V., Ren, Z., Teng, T. Y., Schmidt, M., Ursby, T., Bourgeois, D., Pradervand, C., Schildkamp, W., Wulff, M. & Moffat, K. (2001). *Biochemistry*, **40**, 13802–13815.
Srajer, V., Teng, T. Y., Ursby, T., Pradervand, C., Ren, Z., Adachi, S., Schildkamp, W., Bourgeois, D., Wulff, M. & Moffat, K. (1996). *Science*, **274**, 1726–1729.
Srinivasan, R., Lobastov, V. A., Ruan, C. Y. & Zewail, A. H. (2003). *Helv. Chim. Acta*, **86**, 1763–1838.
Stöhr, J. (1992). *NEXAFS Spectroscopy*. Berlin: Springer.
Tarnovsky, A. N., Gawelda, W., Johnson, M., Bressler, C. & Chergui, M. (2006). *J. Phys. Chem. B*, **110**, 26497–26505.
Thole, B. T., Vanderlaan, G., Fuggle, J. C., Sawatzky, G. A., Karnatak, R. C. & Esteva, J. M. (1985). *Phys. Rev. B*, **32**, 5107–5118.
Tuchagues, J. P., Bousseksou, A., Molnar, G., McGarvey, J. J. & Varret, F. (2004). *Top. Curr. Chem.* **235**, 85–103.
Tyson, T. A., Benfatto, M., Natoli, C. R., Hedman, B. & Hodgson, K. O. (1989). *Physica B*, **158**, 425–427.
Tyson, T. A., Hodgson, K. O., Natoli, C. R. & Benfatto, M. (1992). *Phys. Rev. B*, **46**, 5997–6019.
Vanko, G., Glatzel, P., Pham, V. T. & Bressler, C. (2010). *Phys. Res. B*. Submitted.
Veen, R. M. van der, Milne, C. J., El Nahhas, A., Lima, F. A., Pham, V. T., Best, J., Weinstein, J. A., Borca, C. N., Abela, R., Bressler, C. & Chergui, M. (2009). *Angew. Chem. Int. Ed.* **48**, 2711–2714.
Veen, R. M. van der, Milne, C. J., Pham, V. T., El Nahhas, A., Weinstein, J. A., Best, J., Borca, C. N., Bressler, C. & Chergui, M. (2008). *Chimia*, **62**, 287–290.
Vlcek, A. (2000). *Coord. Chem. Rev.* **200**, 933–977.
Wang, H. X., Peng, G. & Cramer, S. P. (2005). *J. Electron Spectrosc.* **143**, 1–7.
Winter, B. & Faubel, M. (2006). *Chem. Rev.* **106**, 1176–1211.
Zabinsky, S. I., Rehr, J. J., Ankudinov, A., Albers, R. C. & Eller, M. J. (1995). *Phys. Rev. B*, **52**, 2995–3009.
Zewail, A. H. (2000*a*). *Angew. Chem. Int. Ed.* **39**, 2587–2631.
Zewail, A. H. (2000*b*). *J. Phys. Chem. A*, **104**, 5660–5694.
Zewail, A. H. (2006). *Annu. Rev. Phys. Chem.* **57**, 65–103.
Zholents, A. A. & Zolotorev, M. S. (1996). *Phys. Rev. Lett.* **76**, 912–915.